applied sciences

MDPI

Article

Numerical Evaluation of Residual Stress Influence on SIF in CT Specimen

Remigijus Janulionis [1,*] and Gintautas Dundulis [1,2]

[1] Lithuanian Energy Institute, Breslaujos Str. 3, LT-44403 Kaunas, Lithuania; rastine@lei.lt
[2] Kaunas University of Technology, Studentu Str. 56, LT-51424 Kaunas, Lithuania; ktu@ktu.lt
* Correspondence: remigijus.janulionis@lei.lt; Tel.: +370-37-401918

Abstract: Residual stresses are usually associated with stresses induced by heterogeneous deformations as a cause of phase transition and thermal stress. The residual stresses can appear during the manufacturing process, repair process, or in some cases due to operational loads. These stresses should be taken into account in the structural integrity evaluation of low-toughness materials or in the case of fatigue and/or stress corrosion cracking (SCC) situations. Indeed, it is known that residual stresses affect crack growth rates. For a better understanding of how these stresses can interact with crack propagation in pre-strained stainless-steel specimens, numerical modeling has been performed. The tension of the compact tension (CT) specimen was simulated and as a result, the stress intensity factor (SIF) was calculated. The main goal of this paper is to numerically calculate the stress intensity factors along the crack front of the CT specimen with residual stresses and compare them with the results of tension of the same specimen just without residual stresses. For this task finite element analysis (FEA), code CAST3M was used. Simulation results showed that the higher SIF values were calculated at the sides and the lower in the middle part of the CT specimen machined from a highly pre-strained plate which is opposite to what could be expected in a specimen without residual stresses.

Keywords: residual stresses; fracture mechanics; stress intensity factor; finite element method; FEM; SIF

Citation: Janulionis, R.; Dundulis, G. Numerical Evaluation of Residual Stress Influence on SIF in CT Specimen. *Appl. Sci.* **2023**, *13*, 6180. https://doi.org/10.3390/app13106180

Academic Editor: Alberto Campagnolo

Received: 19 April 2023
Revised: 12 May 2023
Accepted: 16 May 2023
Published: 18 May 2023

1. Introduction

The main reasons for the failure of the steel components and pipelines at nuclear power plants are the defects that appear during the manufacturing processes or operation. The defects usually are cracks that appear due to material degradation mechanisms such as stress corrosion cracking (SCC), fatigue, or others. Material, stresses, and environment are the three factors that should be present in order for SCC to initiate. All these factors are important and, in some cases, could lead to the formation of a crack [1,2]. This kind of defect usually appears in pipe welds at heat-affected zones. Undetected and unevaluated cracks are very dangerous because they can lead to fast failure or even to the guillotine break of the pipelines and other pressure vessels at relatively low loading conditions. Therefore, it is very important to detect and evaluate these defects. Casting, rolling, bending, pressing, stamping, welding, and other manufacturing processes lead to the accumulation of residual stresses which also have to be taken into account. It is known that residual stresses affect crack growth rates [3–5] and the durability under the effect of cyclic loading [6–10]. Residual stresses and weld defects together have critical and risky effects on the structures. The static residual stresses have an influence on the life of components under fatigue loading conditions. These variations are introduced in both initiation and growth of fatigue cracks [11].

SIF is important for the evaluation of crack initiation and growth. Cracks usually appear in the weld seams or heat-affected zones where welding residual stress is present. Acting operational stresses together with residual stress could lead to unpredicted/premature

weld seam failure. Therefore, it is important to know how the residual stress affects crack initiation and growth in the structural integrity analysis of weld seams. In this research, thermal loading was applied to the finite element (FE) model for the introduction of residual stress and evaluation of their influence on SIF values.

Despite the significance of residual stresses, there has not been much research on the effects of combining crack closure mechanisms with residual stress distributions during crack propagation. Since both tension and compression stress values are present across the thickness, the crack closure can be described using the polynomial equation [7]. The main reasons for the rare investigation of the residual stress effect could be the difficult and long-lasting experimental stress measurements. Furthermore, it is difficult to predict the residual stresses accurately that arise from manufacturing procedures. Typically, in such cases, a nonlinear FE analysis is used. Due to the lack of accurate residual stress data in the components and structures, the integrity analysis based on fracture mechanic analysis is usually limited or too conservative. As a result, residual stress-bearing structures' structural integrity is evaluated cautiously, frequently, and very conservatively which frequently forces safe equipment out of service earlier than necessary and at a large expense [12].

According to this, it is important to estimate the influence of the residual stress on the behavior of defects in welded structures. Lee and Chang [13] using FEA analyzed how the defects in welds affect the cylindrical steel members structurally. As a result, non-axisymmetric buckling was determined close to regions with defects caused by an asymmetric distribution of residual stress. Labeas and Diamantakos [14] evaluated the weld residual stresses for cracked T-joints welded with a laser beam and calculated the stress intensity factor (SIF) using FEA with different crack shapes. The damage tolerance methodology was used for the determination of the weld joint's remaining lifetime. Lee and Chung [15] conducted a numerical non-linear 3D analysis to determine the residual stresses on welds of similar as well as dissimilar metals. It was concluded that the difference between the longitudinal residual stresses increases together with the yield strength of the parent materials in dissimilar steel welds. Wu [16] evaluated the residual stresses effect on a surface crack with a brittle fracture behavior. He recommended a post-heat treatment to relax the residual stress in the weld joints.

In trying to understand what influence makes residual stresses on austenitic stainless steels and how they interact with the initial level of pre-straining, research work was carried out in the CEA Saclay, France [17]. The SCC resistance of the initially pre-strained plate (from 30% to 60%) was analyzed in these experiments. To carry out such an experiment, the CT specimen was machined from the pre-strained plate. Before the SCC test, a fatigue pre-cracking is performed on each specimen. At the end of the SCC tests, the CT specimen was completely broken by using the testing machine. The fracture surface revealed a particular fatigue crack with a smaller propagation at the center of the specimen and no SCC crack growth at this location, whereas significant SCC propagation has been obtained near the edges.

The numerical simulation of the stress intensity factors along the crack front of the CT specimen was carried out. Usually research is made for a not pre-strained material on a specimen with an initial straight crack front or machined notch, and the higher values of the stress intensity factor are observed in the middle of the specimen and lower values are observed at the sides of the specimen: a larger crack growth in the middle of the specimen is then expected, which was not the case here. However, in the case when the plate was initially pre-strained (plate with residual stresses), it seems that an opposite distribution of stress intensity factor along the crack front is observed: the higher values were at the sides of the specimen and the lower ones were in the middle. It was also justified by the obtained crack shape after pre-cracking.

The main goal of this paper is to numerically evaluate how the residual stress affects the SIF profile at the crack front. To achieve the main goal of the research, the following tasks should be conducted:

1. create the residual stress profile in the numerical model by adding a temperature profile;
2. apply the created residual stress profile to the standard CT specimen model;
3. compare the numerically determined SIF profile in cases with and without residual stress.

To accomplish the previously described tasks, the computer program Cast3M was chosen [16]. This program is based on the FEM which is validated for the calculation of fracture parameters such as SIF and J-integral. To make this research close to a real-life scenario, the experimentally determined material properties and the measured residual stress profile of highly pre-strained stainless-steel plates were used. The experimental tests and FE simulation were conducted at an elevated 325 °C temperature.

The analysis results of this research show how residual stresses affect the SIF profile along the crack front and that these stresses have a bigger influence on the surface rather than the central part of the specimen. As the secondary goal of the paper, the method for residual stress application to the FE model was demonstrated.

2. Initial Data for FEA

The preparation of specimens, mechanical properties, and all the experiments were carried out at Atomic Energy Research Center (CEA Saclay), France [17].

The tests were made using the CT specimen machined from a pre-strained 316 L stainless steel plate. The plate was pre-strained at about 40% in the T (transverse) direction (see Figure 1). Pre-straining was made by rolling in RD direction (rolling direction). TRD (transverse rolling direction) is a perpendicular direction to RD. Due to rolling at a high strain level, the otherwise straight plate was curved, where one surface of the plate became concaved and the other—convexed. The plate thickness after rolling was ~20 . . . 21 mm and the machined CT specimen's thickness was 15 mm.

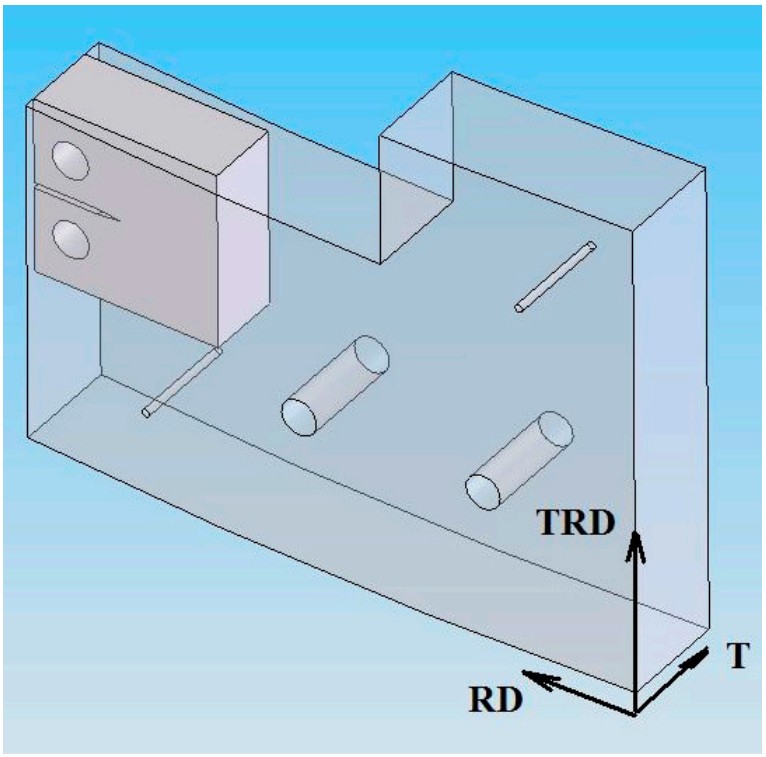

Figure 1. Pre-strained plate with CT specimen.

The same plate was used for residual stress measurement performed by Bristol University [17] using their developed deep hole drilling (DHD) technique [18]. The measurement technique consists of four steps. Initially, a small diameter hole is drilled through the thickness of the measured specimen. The second step is the accurate measurement of the diameter of this hole at many depths and angular points. After that, the material around the hole is freed coaxially using a coring tool. The last step consists of the measurement of the hole diameter at the same measurement points as in the second step. The measured distortion of the diameter is later used for the determination of residual stress. Measured residual stress profiles are shown in Figure 2. The figure shows the residual stress distribution along the thickness of the plate in RD and TRD directions. The distance of 0 mm is on the convex surface of the plate (see Figure 3) and the distance of 20 mm is on the opposite (concave) surface. The measurements show the higher residual stresses are in TRD, the same direction CT specimen tension, and crack opening is simulated. Therefore, residual stresses in TRD will be taken into account in this analysis.

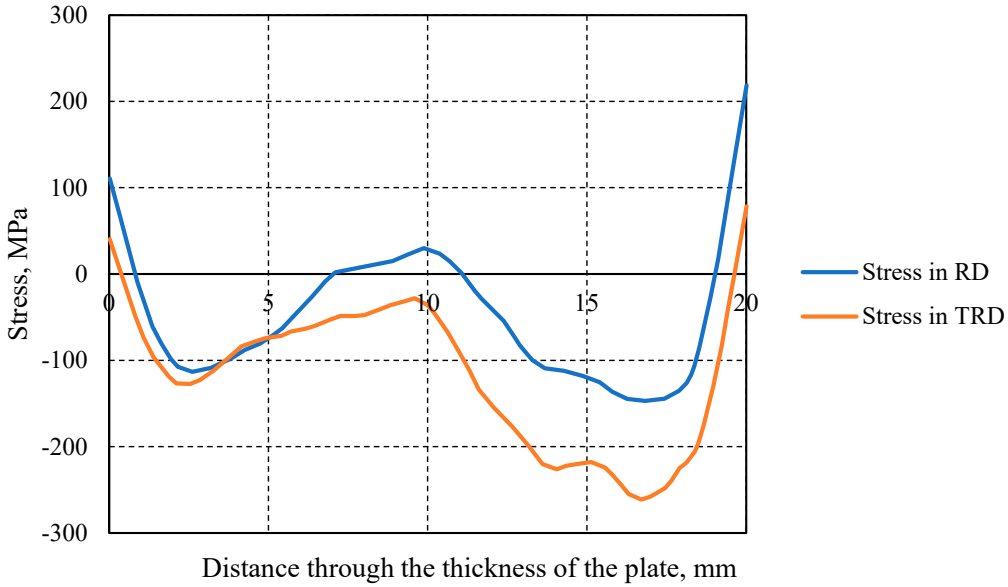

Figure 2. The profiles of measured residual stresses.

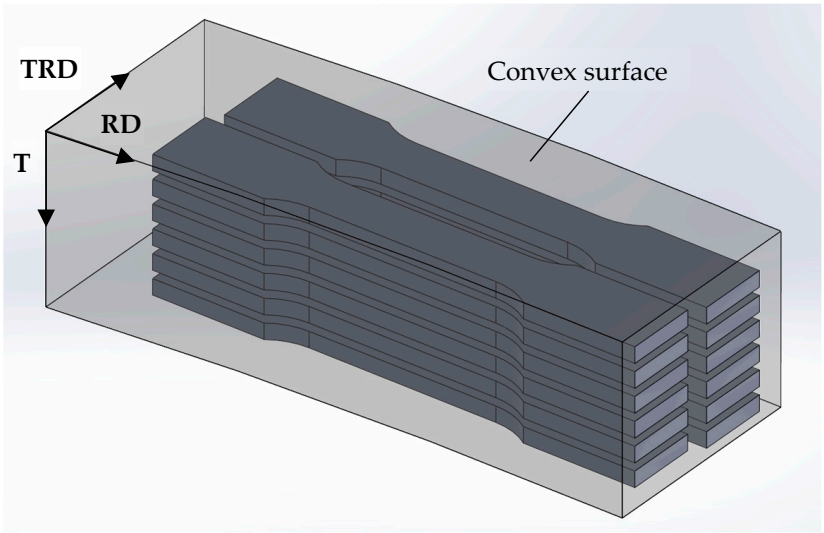

Figure 3. Location and orientation of the tensile specimen in the plate.

The tensile testing of 316 L stainless steel was made at 325 °C. The location and orientation of the tested tensile specimens in the plate are shown in Figure 3. Two columns with six specimens in each column in different plate depths were prepared. In total, twelve 2 mm thickness specimens were tested. The averaged material properties are as follows [17]:

- Modulus of elasticity E = 176,360 MPa,
- Poisson's ratio ν = 0.3,
- yield stress Rp0.2 = 655 MPa,
- cinematic stress hardening H = 20 GPa,
- thermal expansion coefficient $\alpha = 1 \times 10^{-5}/°C$.

3. Residual Stress Modeling

The original stainless-steel plate was pre-strained by rolling at very high ratios (between 30% and 60%). In fact, the pre-straining was not homogeneous through the thickness, which generated a residual stress profile to ensure strain compatibility. In this paper, the focus will be on the plate pre-strained at 40%.

There is no straightforward method for residual stress application at the numerical model in most FEA codes. It is not always possible to obtain a correct distribution of residual stresses using only external mechanical loading, such as force or pressure. That is why, in this case, thermal loading was used. It was based on the assumption that thermal loading and residual stresses are equivalent to the imposed strain loading conditions. The change in the temperature compared to the base temperature makes the material expand or contract. The amount of expansion is described in the material model by the thermal expansion coefficient. Temperature itself cannot induce stress or strain if the expansion or contraction of the material is not restricted. Only then, if the expansion or contraction is restricted, can the strain in the material appear. The restriction in the model can be applied by the boundary conditions or by the opposite thermal load similar to the forces acting in opposite directions. According to this, we applied the temperature profile to the model in such a way that the induced stress profile was similar to the measured residual stresses. In addition, this obtained stress profile was used for the evaluation of residual stress influence on SIF.

The main challenge of thermal load application is to find the correct temperature profile distribution through the thickness of the plate which leads to a similar residual stress distribution that was measured experimentally. The next step is to run the CT specimen tension simulation for SIF calculation by applying the defined temperature distribution.

For the determination of the thermal profile for residual stress application and SIF calculation, the FE code Cast3M was used. This code was developed in DEN/DM2S/SEMT CEA Saclay, France and is used for solving various problems, especially for fracture mechanics [19].

3.1. FE Model for the Residual Stress Modeling

To find the correct temperature distribution along the thickness of the steel plate, the FE model of the 20 mm thick plate was made (see Figure 4). The modeled steel plate was three times bigger than the CT specimen and its dimensions were 90 × 90 × 20 mm. The three-dimensional cubic elements CU20 were used for the mesh of the plate which have 20 nodes.

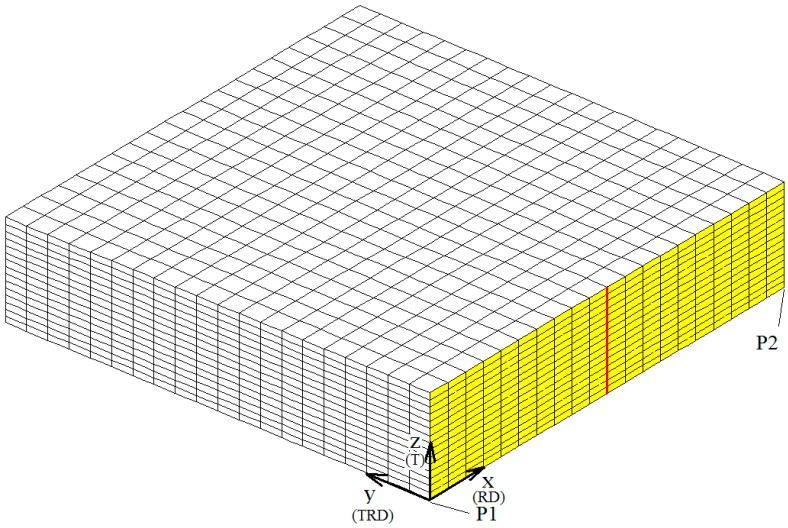

Figure 4. Simple FE model.

For the residual stress distribution calculation, an elastic analysis was conducted. Therefore, to describe the material only, the modulus of elasticity, Poisson's ratio, and thermal expansion coefficient presented in Section 2 were used.

The following boundary conditions of the model were applied: the displacements of point P1 were restrained in all three directions; the displacement of point P2 was restrained along the *Z* axis; the displacement of the yellow-colored surface was restrained along the *Y* axis (see Figure 4).

The red-colored line is the line where the stress profile was measured.

3.2. Results of the Residual Stress Modeling

To find the correct temperature profile which results in a stress profile similar to the measured one (Figure 2), several calculations were conducted. As was explained in Section 3 in order to induce stress using thermal loading, the temperature profile should have lower and higher values according to base temperature. For convenience, the base temperature of the material was selected to be equal to 0 °C which is a temperature at which no stresses are induced. The measured residual stresses have the compressive and tensile stresses, therefore, the thermal load should also have lower and higher values compared to the base temperature equal to 0 °C. In our case that would be negative and positive temperature values. Positive thermal load values force the material to expand. Without restriction, only the dimensions of the model would increase, and no stresses would appear. The restrictions to the expansion of the material were applied by negative temperature values. The restriction to the expansion of the material induces compressive stress, and vice versa, restriction to the contraction of the material induces tensile stress. That is why the temperature profile should look somewhat like a mirror image of the residual stress profile in respect to the abscissa of the graph. Moreover, to avoid the warping of the model temperature profile, there should be symmetry along the middle plane of the model.

Taking into account all the statements, the above temperature profile was constructed. The actual temperature values were adjusted by running several FE analyses and comparing the calculated stress profile with the measured residual stresses.

The best temperature profile found is shown in Figure 5. The figure also shows the trendline and a polynomial equation describing the profile. The best-fit temperature profile shows the lowest temperature values up to −200 °C on the surfaces of the plate, and the highest values up to 200 °C in 5.5 mm depth from both surfaces of the plate.

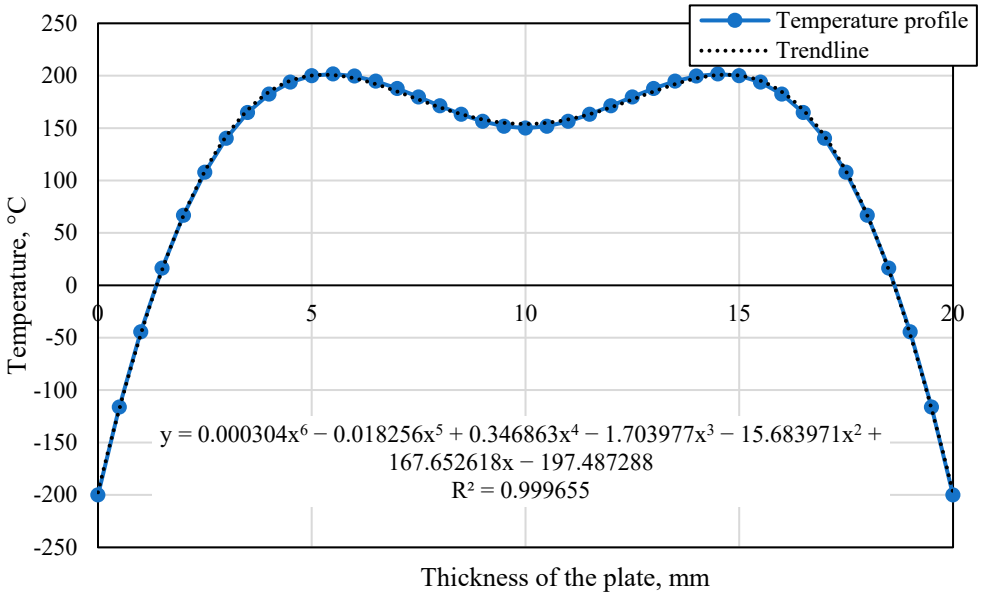

Figure 5. Temperature profile.

The found temperature profile was applied to the plate as the loading (see Figure 6). The temperature was applied to all nodes of the model where the temperature value for each node was calculated according to the following equation:

$$T = 0.000304 \cdot z^6 - 0.018256 \cdot z^5 + 0.346863 \cdot z^4 - 1.703977 \cdot z^3 - 15.683971 \cdot z^2 + 167.652618 \cdot z - 197.487288, \quad (1)$$

here, T—temperature, °C; z—z coordinate of the node, mm.

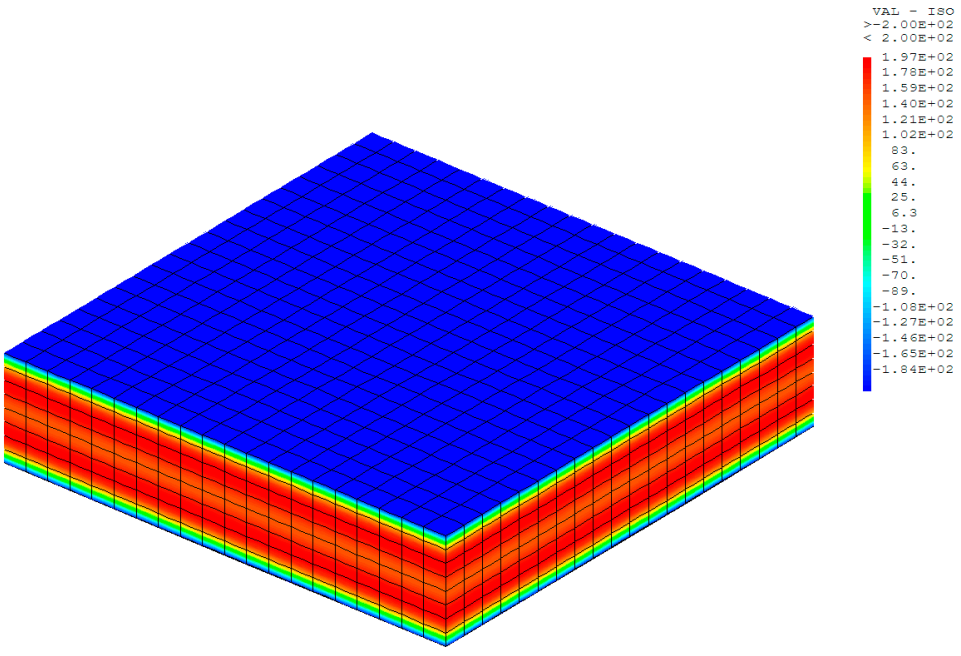

Figure 6. Temperature loading distribution through the thickness of the plate (°C).

Von Misses stress distribution due to the temperature loading is shown in Figure 7 and the stress profile in TRD is shown in Figure 8. The obtained stress profile has the simplified shape of the measured residual stress profile. The lowest stress values are −200 MPa; in the very middle of the plate, the stress value is −50 MPa and the highest values are up to 800 MPa on both sides of the plate. As we are interested in SIF calculation, evaluating

residual stress in the CT specimen, which is 15 mm thick in the very ends of the stress profile, is not important. The 2.5 mm of the plate from both sides as well as the thermal loading profile will be cut out. Moreover, the exact match of the residual stress of the profile is not relevant in the current study because the final results, i.e., SIF profile, will not be measured with experimental data, but only with the numerically determined SIF profile in cases with and without residual stress profile. It is because standard procedures for experimental determination give an average value of SIF through the thickness of the specimen but not a profile.

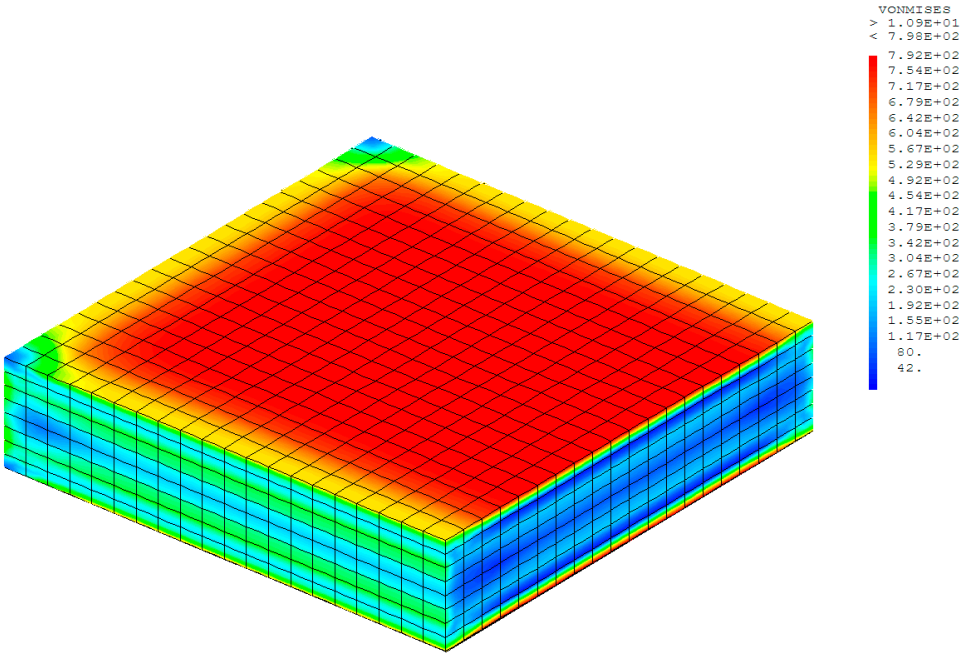

Figure 7. Von Misses stress distribution in the plate (MPa).

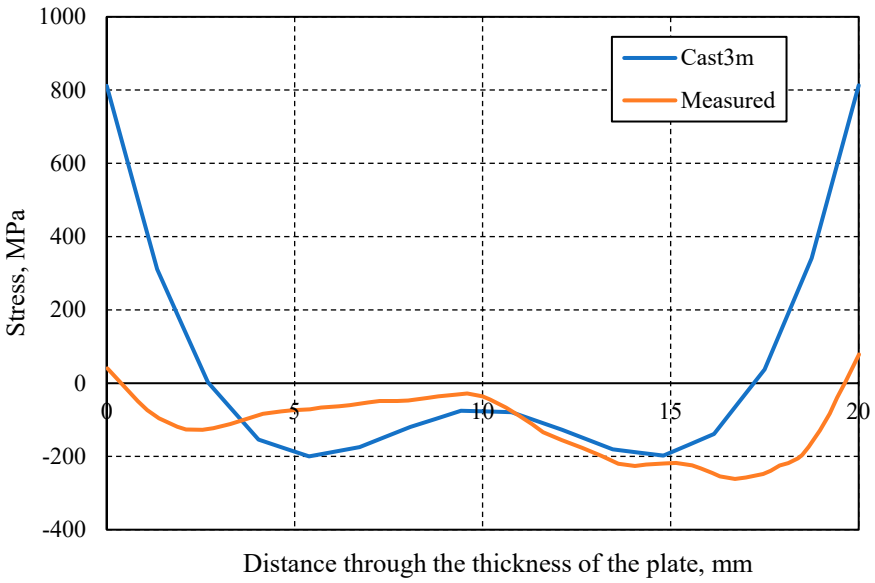

Figure 8. Stress profile in the plate (direction TRD).

To find out what the residual stress profile will be in the CT specimen when the cut out thermal profile is applied to the model, the calculation was performed, and the results are presented in Section 4.2.

4. Stress Intensity Factor Calculation

4.1. FE Model for the Stress Intensity Factor Calculation

The FE model of the CT specimen with a straight crack front was created for the calculation of the SIF. Due to the symmetric geometry of the CT specimen, only half of the model was created (see Figure 9). The same FE CU20 as for the stainless-steel plate was used in this model. In order to obtain high calculation precision of the SIF calculation, the mesh of small elements around the crack tip was created. Using this CT specimen FE model, three cases were analyzed: residual stress analysis and two cases for SIF analysis with and without residual stress. The different load combinations were used for these cases:

- previously find temperature distribution for residual stress calculation;
- displacement for stress intensity factor calculation;
- previously find temperature distribution and displacement for stress intensity factor calculation with residual stress.

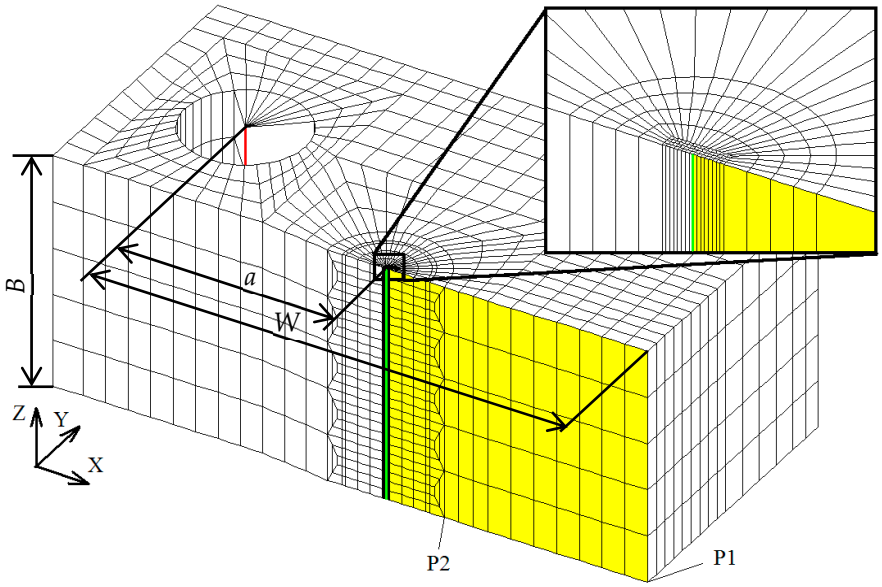

Figure 9. FE mesh of CT specimen.

The displacement load of 40 μm (or 80 μm for full-scale model) along the coordinate Y was used. As displacement imitates the movement of the pin of the testing machine, it was applied on the red-colored line shown in Figure 9.

The following boundary conditions of the model were used: displacement of point P1 was restrained in all three directions; displacement of point P2 was restrained along the *Z* axis; displacement of the yellow-colored surface was restrained along the *Y* axis which imitates the symmetric boundary condition.

The green-colored line is the crack front and the line where the stress profile is shown.

An elastic calculation was used for residual stress analysis and elastic—plastic with kinematic hardening calculations were used for other cases.

The material properties presented in Section 2 were used to describe the material behavior of the CT specimen model.

4.2. Results of Residual Stress and Stress Intensity Factor Calculation

The first analysis was the analysis of residual stresses. Obtained stress profile (see Figure 10) is shown on the crack front. The stress profile in the CT specimen has a similar shape as the stress profile in the plate (see Section 3) but the actual values are different. In this case, the lowest stress value is −73 MPa, in the middle of the CT specimen the stress reaches 43 MPa, and at both surfaces, stress values are 193 MPa. The residual stress value difference in the CT specimen compared to the plate model can be explained as a

stress relaxation in the steel after machining the CT specimen and cutting out high-stress outer layers of the plate. When the CT specimen was machined from the pre-strained steel plate, 2.5 mm of the material together with high stresses were cut from both sides. After that, the inner compressed volumes of the steel were constrained by lower surface tension stresses and the steel could relax reducing inner volume compression. The distribution of the crack opening stress σ_y (direction TRD) in the CT specimen is presented in Figure 11. To understand how SIF distributes along the crack front due to residual stress, the SIF calculation was conducted.

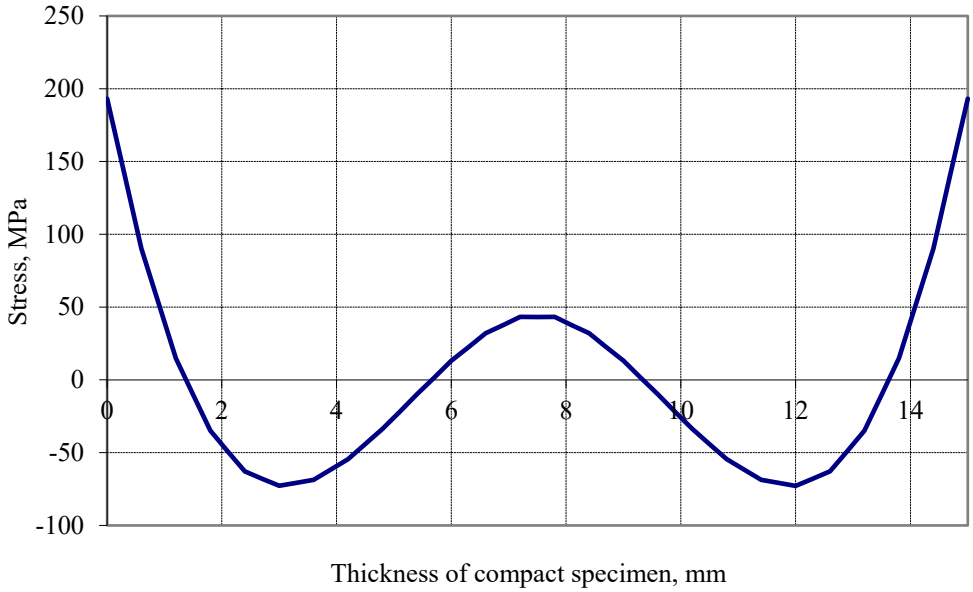

Figure 10. Stress profile in the CT specimen (direction TRD).

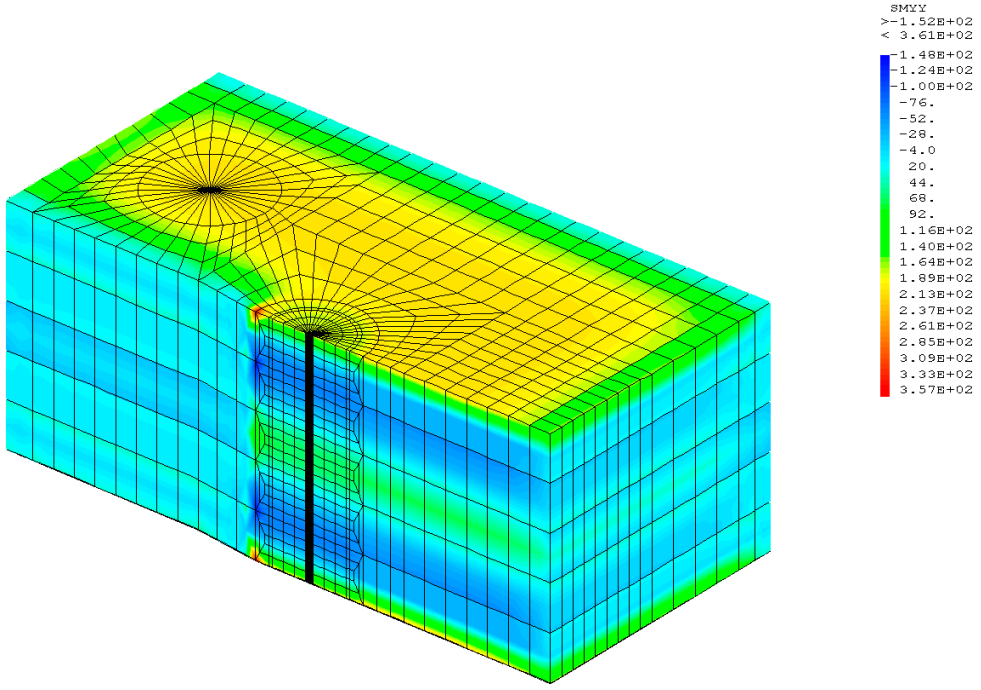

Figure 11. Distribution of crack opening stress σ_y (direction TRD) at residual stress case (MPa).

According to ASTM E399-12e3 standard [20], using standard shape and size specimen, SIF can be calculated analytically by the following equation:

$$K_I = \left(P_Q / BW^{1/2}\right) \cdot f(a/W) \quad (2)$$

where:

$$f(a/W) = \frac{\left(2 + \frac{a}{W}\right)}{\left(1 - \frac{a}{W}\right)^{3/2}} \cdot \left[0.886 + 4.64\frac{a}{W} - 13.32\left(\frac{a}{W}\right)^2 + 14.72\left(\frac{a}{W}\right)^3 - 5.6\left(\frac{a}{W}\right)^4\right] \quad (3)$$

here: K_I—stress intensity factor, MPa·m$^{0.5}$; P_Q—load, N; B –specimen thickness, m; W—specimen width, m; a—crack length, m (see Figure 9).

However, as it was proven earlier [21], FE programs usually have fairly accurate built-in scripts for numerical SIF calculation. Therefore, in this study, numerical simulation of SIF was chosen. For the accuracy verification of the created FE model, the comparison of numerically and analytically calculated SIF was conducted. The results are shown in Figure 12. As can be seen, numerically determined SIF values are a little bit higher than those calculated analytically using Equations (2) and (3). However, the difference is fairly small, and at 6 kN, load is around 3%. The load around 5800 N is reached at the crack opening displacement of 40 μm (or 80 μm for full-scale model).. According to the results, it can be concluded that the created FE model is sufficiently accurate and can be used for SIF calculation.

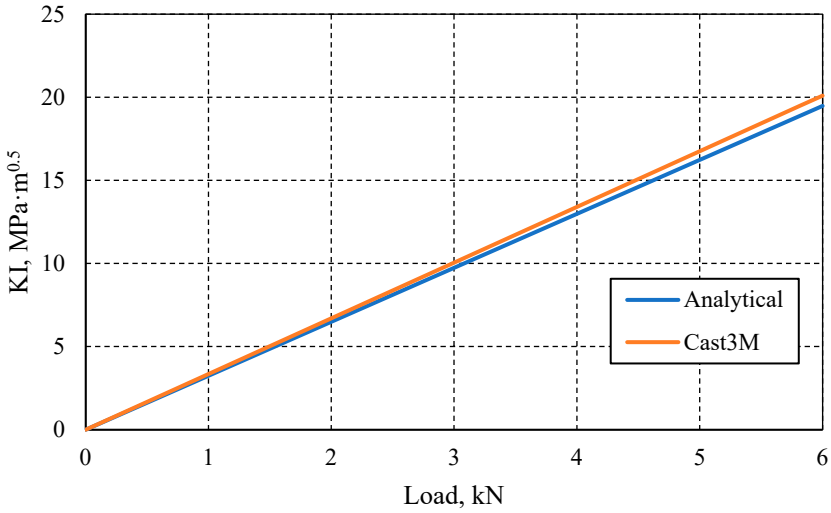

Figure 12. Comparison of analytical and numerical calculation of SIF.

The obtained numerically determined SIF results are presented in Figure 13. The figure shows that the shape of the SIF profile matches the shape of the stress profile. The SIF values reach 3.6 MPa·m$^{0.5}$ on both sides of the specimen. However, deeper in the middle layers of the specimen, the SIF becomes negative. The lowest SIF value is −10.6 MPa·m$^{0.5}$, but in the very middle of the specimen, it is slightly higher and reaches −5.4 MPa·m$^{0.5}$. SIF is usually associated with the crack opening due to tension load and tension stress. In our case, residual stresses are both tensile and compressive. Compressive stress acts in the opposite way, i.e., tries to close the crack. In reality, crack closure would stop at the point when two crack surfaces meet each other. However, in our model, for simplification, only half of the CT specimen is created and no contact of the crack surface to a symmetry plane is modeled. Therefore, due to compressive residual stress, the crack surface can deform much more and pass the symmetry plane which results in negative SIF values. Negative SIF values do not have much of a meaning, but, as these are only intermediate results,

they can be ignored. The crack closure effect will be much more important when the CT specimen under tension is analyzed.

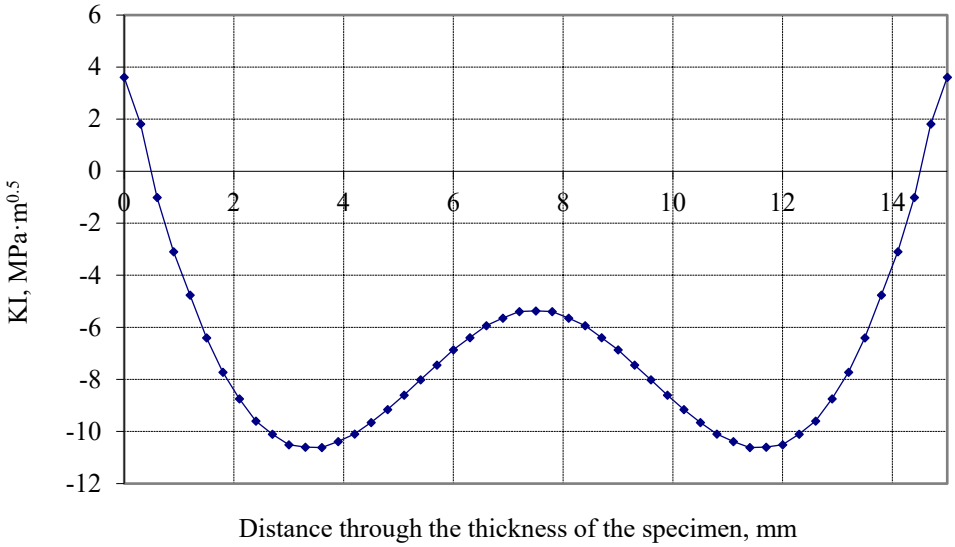

Figure 13. Stress intensity factor values through the thickness of the specimen due to residual stress.

Finally, the last two cases were analyzed: SIF calculation with and without residual stress. The distributions of crack opening stress σ_y for the case with residual stress is shown in Figure 14. The highest stresses were obtained at the crack tip.

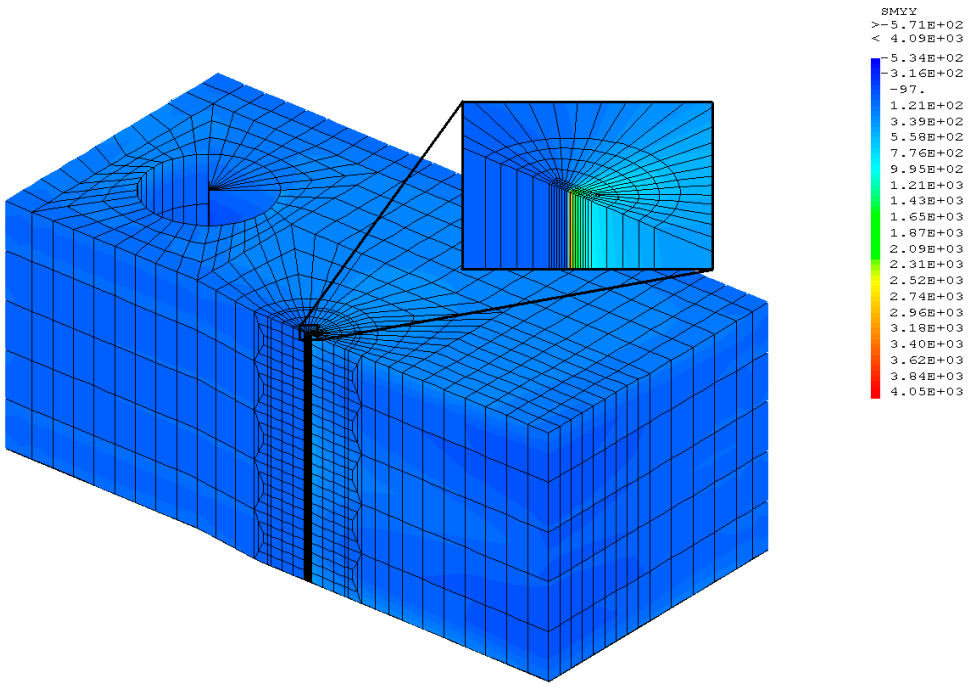

Figure 14. Distribution of crack opening stress σ_y (direction TRD) in loading case with residual stress (MPa).

FEA results of SIF calculation through the thickness of the specimen with and without residual stress load cases are shown in Figure 15.

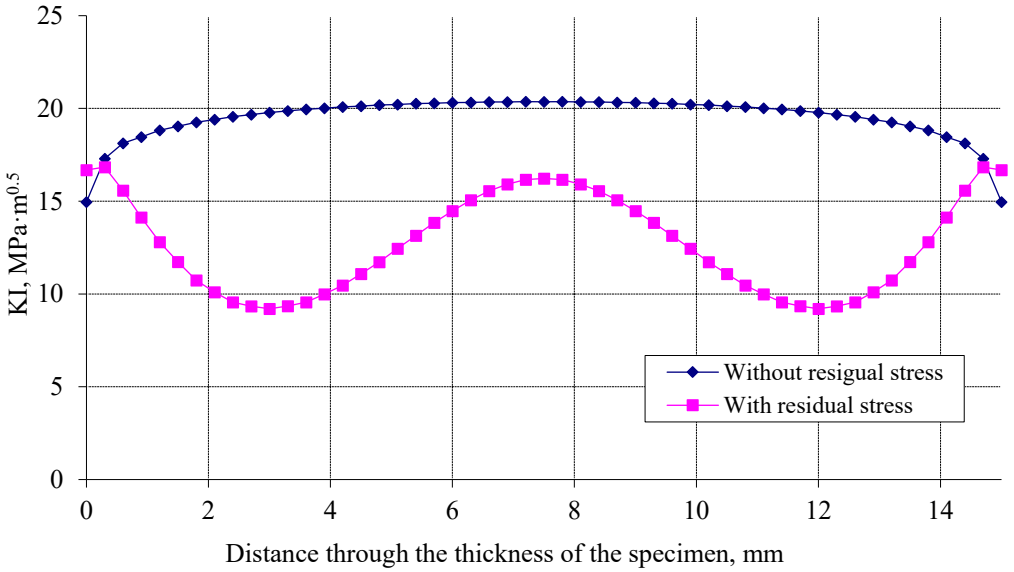

Figure 15. Stress intensity factor values through the thickness of the specimen with and without residual stress.

As it is shown in Figure 15, the SIF values for the load case without residual stresses are 14.9 MPa·m$^{0.5}$ at both sides of the CT specimen and 20.3 MPa·m$^{0.5}$ in the middle of the specimen, i.e., lower values are at the sides and higher in the middle. However, the results are opposite in the loading case with the residual stresses, where SIF values at the side surfaces are 16.7 MPa·m$^{0.5}$ and in the middle is 16.2 MPa·m$^{0.5}$. The reason for the lower values of K_I in the case with the residual stresses is the dominant compression stress in the residual stress profile which compensates for the stress occurring due to tension load. As a consequence, the values of K_I decreased and matched the shape of the residual stress profile.

Such an unusual increase in K_I values is dangerous from the crack propagation perspective, especially for stress corrosion cracking mechanism as, due to a corrosive environment, such cracks tend to form and propagate from the free surface of material [17].

5. Conclusions

In the current research, the following analyses were conducted:

- residual stress modeling by finding the temperature profile which leads to the stress profile similar to the measured;
- stress intensity factors in CT specimen calculation and comparison at loading cases with and without residual stresses.

The results of the analysis have shown that in particular cases, the residual stresses can lead to a situation where the values of the stress intensity factor at the middle of the specimen are lower than at the sides. That should be taken into account when surface cracks and their propagation is evaluated. Moreover, in the analyzed case, residual stresses have reduced the average value of the stress intensity factor. However, in the case of different residual stress profiles, the result could be the opposite, i.e., the average stress intensity factor value could be increased due to residual stresses, which is usually observed in weld seams. Therefore, residual stresses should always be evaluated and cannot be neglected.

The methodology of this analysis can be used in the structural integrity evaluation of defects in metal components with residual stresses. It is important to note that the methodology is designed to create a residual stress profile using temperature as loading and evaluate the influence of residual stress on SIF. The calculation accuracy is very much dependent on the correct thermal load profile determination. As it does not allow for determining the residual stresses numerically, great attention should be paid to the residual

stress measurement, thermal load determination, and model calibration. The main drawback of the method is the destructive nature of residual stress measurements. To improve that, new non-destructive methods should be used.

Author Contributions: Methodology, R.J.; Validation, G.D.; Formal analysis, R.J.; Writing—original draft, R.J.; Writing—review & editing, G.D.; Supervision, G.D. All authors have read and agreed to the published version of the manuscript.

Funding: This research received no external funding.

Institutional Review Board Statement: Not applicable.

Informed Consent Statement: Not applicable.

Data Availability Statement: Not applicable.

Acknowledgments: The authors would like to express gratitude to the administration and scientists of Atomic Energy Commission CEA-Saclay for providing information regarding the carried out research. We would like to express special thanks to Stephane Marie, a former head of the Systems and Structures Modeling Department at CEA Saclay.

Conflicts of Interest: The authors declare no conflict of interest.

References

1. IAEA. *IAEA Extrabudgetary Programme on Mitigation of Intergranular Stress Corrosion Cracking in RBMK Reactors*; Working Group 2 on Comprehensive Assessment Techniques; Final Report; IAEA: Vienna, Austria, 2002.
2. Djarot, D.B.; Gapsari, F.; Lobo, O.B.; Simanjuntak, F.M. Stress Corrosion Cracking Threshold for Dissimilar Capacitive Discharge Welding Joint with Varied Surface Geometry. *Appl. Sci.* **2020**, *10*, 2180. [CrossRef]
3. Xin, H.; Veljkovic, M. Residual stress effects on fatigue crack growth rate of mild steel S355 exposed to air and seawater environments. *Mater. Des.* **2020**, *193*, 108732. [CrossRef]
4. Ribeiro, V.; Correia, J.; Mourão, A.; Lesiuk, G.; Gonçalves, A.; Jesus, A.; Berto, F. Fatigue crack growth modelling by means of the strain energy density-based Huffman model considering the residual stress effect. *Eng. Fail. Anal.* **2022**, *140*, 106543. [CrossRef]
5. Cao, B.; Cheng, S.; Li, A.; Deng, Y.; Fang, Z. Fatigue Crack Propagation Study of Bridge Steel Q345qD Based on XFEM Considering the Influence of the Stress Ratio. *Appl. Sci.* **2022**, *12*, 12782. [CrossRef]
6. Lee, C.H.; Chang, K.H. Finite element computation of fatigue growth rates for mode I cracks subjected to welding residual stresses. *Eng. Fract. Mech.* **2011**, *78*, 2505–2520. [CrossRef]
7. Al-Mukhtar, M. Residual Stresses and Stress Intensity Factor Calculations in T-Welded Joints. *J. Fail. Anal. Prev.* **2013**, *13*, 619–623. [CrossRef]
8. Schnubel, D.; Huber, N. The influence of crack face contact on the prediction of fatigue crack propagation in residual stress fields. *Eng. Fract. Mech.* **2012**, *84*, 15–24. [CrossRef]
9. Kacianauskas, R.; Zenon, M.; Zarnovskij, V.; Stupak, E. Three-dimensional correction of the stress intensity factor for plate with a notch. *Int. J. Fract.* **2005**, *136*, 75–98. [CrossRef]
10. Guerre, C.; Raquet, O.; Herms, E.; Le Calvar, M.; Turluer, G. SCC growth behaviour of austenitic stainless steels in PWR primary water conditions. In Proceedings of the 12th International Conference on Environmental Degradation of Materials in Nuclear Power Systems—Water Reactors, Salt Lake City, UT, USA, 14–18 August 2005; pp. 1029–1036.
11. Seifi, R. Effect of Residual Stress on Fracture Parameters of through Cracks in Welded Plates. *Procedia Eng.* **2011**, *10*, 1895–1900. [CrossRef]
12. Coules, H.E.; Smith, D.J. The maximum possible stress intensity factor for a crack in an unknown residual stress field. *Int. J. Press. Vessel. Pip.* **2015**, *134*, 33–45. [CrossRef]
13. Lee, C.H.; Chang, K.H. Influence of the residual stresses and distortions on the structural behaviour of girth-welded cylindrical steel members. *J. Constr. Build. Mater.* **2013**, *41*, 766–776. [CrossRef]
14. Labeas, G.; Diamantakos, I. Laser beam welding residual stresses of cracked T-joints. *J. Theor. Appl. Fract. Mech.* **2013**, *63–64*, 69–76. [CrossRef]
15. Lee, C.H.; Chang, K.H. Numerical analysis of residual stresses in welds of similar or dissimilar steel weldments under superimposed tensile loads. *J. Comput. Mater. Sci.* **2007**, *40*, 548–556. [CrossRef]
16. Wu, X.R. The effect of welding residual stress on brittle fracture of plates with surface cracks. *J. Eng. Fract. Mech.* **1984**, *19*, 427–439. [CrossRef]
17. Marie, S.; Guerre, C.; Herms, E. Analysis of the truth loading conditions of a austenitic CT specimen during a SCC experiment. In Proceedings of the 2011 ASME PVP Conference, Baltimore, MD, USA, 17–21 January 2011. [CrossRef]

18. Mirzaee-Sisan, A.; Fookes, A.J.; Truman, C.E.; Smith, D.J.; Brown, T.B.; Dauda, T.A. Residual stress measurement in a repair welded header in the as-welded condition and after advanced post weld treatment. *Int. J. Press. Vessel. Pip.* **2007**, *84*, 265–273. [CrossRef]
19. Cast3m. Available online: http://www-cast3m.cea.fr/ (accessed on 12 October 2022).
20. *ASTM E399-12e3*; Standard Test Method for Linear-Elastic Plane-Strain Fracture Toughness KIc of Metallic Materials. American Society of Testing and Materials: West Conshohocken, PA, USA, 2018. [CrossRef]
21. Janulionis, R.; Dundulis, G.; Grybėnas, A. Numerical Research of Fracture Toughness of Aged Ferritic-Martensitic Steel. *Metals* **2020**, *10*, 1686. [CrossRef]